catalysts

MDPI

Article

Catalytic Oxidation of Chlorobenzene over Ruthenium-Ceria Bimetallic Catalysts

Meng Ye [1,*], Li Chen [2,3], Xiaolong Liu [2], Wenqing Xu [2], Tingyu Zhu [2] and Guanyi Chen [1]

1 School of Environmental Science and Engineering, Tianjin University, Tianjin 300072, China; chen@tju.edu.cn
2 Beijing Engineering Research Center of Process Pollution Control, National Engineering Laboratory for Hydrometallurgical Cleaner Production Technology, Institute of Process Engineering, Chinese Academy of Sciences, Beijing 100190, China; chenli@ipe.ac.cn (L.C.); liuxl@ipe.ac.cn (X.L.); wqxu@ipe.ac.cn (W.X.); tyzhu@ipe.ac.cn (T.Z.)
3 Chemistry and Chemical Engineering, Guizhou University, Guiyang 550025, China
* Correspondence: mye@ipe.ac.cn; Tel.: +86-10-8254-4823

Received: 28 February 2018; Accepted: 13 March 2018; Published: 16 March 2018

Abstract: A series of Ru-based mono and bimetallic materials were prepared and evaluated in the catalytic oxidation of chlorobenzene. Among the different Ru-based catalysts, $1Ru/TiO_2$(P25) was the most active catalyst and contributed the lowest complete oxidation temperature, suggesting that commercial P25 TiO_2 was the best support for Ru catalysts. After ceria oxides were introduced into the Ru catalytic system, the catalytic activity of $1Ru\text{-}5Ce/TiO_2$(Rutile) dramatically improved and that of P25 supported catalysts was decreased. Comparing the chlorobenzene consumption rates for $1Ru/TiO_2$ and $1Ru\text{-}5Ce/TiO_2$ at 280 °C, it could be concluded that monometallic Ru catalytic system was appropriate for P25 support, and the Ru-Ce bimetallic catalytic system was suitable for the rutile TiO_2 support. At 280 °C, for $1Ru\text{-}5Ce/TiO_2$(Rutile) and $1Ru\text{-}5Ce/TiO_2$(P25), the chlorobenzene conversion was stabilized at approximately 91% and 86%, respectively. According to the physicochemical properties of the catalysts as characterized by X-ray diffraction (XRD), X-ray photoelectron spectroscopy (XPS), transmission electron microscopy (TEM), high-angle annular dark-field scanning transmission electron microscopy (HAADF-STEM), and Hydrogen temperature programmed reduction (H_2-TPR), it can be concluded that (a) electrophilic O_{ads} species play an important role in VOCs oxidation; (b) abundant RuO_2 nanoparticles on the surface of $1Ru\text{-}5Ce/TiO_2$(Rutile) result in higher catalytic activity and stability; and (c) dispersion is not the major factor for the catalytic activity, rather the unique structure greatly facilitated the catalytic activity and stability.

Keywords: chlorinated volatile organic compounds; chlorobenzene; catalytic oxidation; ruthenium; bimetallic catalysts

1. Introduction

Reducing volatile organic compounds (VOCs) emissions has been a major challenge for manufacturers and researchers [1,2]. In comparison to other VOCs, chlorinated volatile organic compounds (CVOCs) are more toxic and difficult to remove from the flue gas [3–6]. Many strategies have been developed for CVOC abatement, including incineration, catalytic oxidation, and adsorption-based techniques [7–9]. Among those methods, catalytic oxidation has been regarded as the most promising due to its advantages of high efficiency and absence of secondary pollution [7,10–12].

Numerous catalysts have been reported for CVOC purification, with the research mainly focused on the noble metals [13–17] and transition metal oxides [18–27]. Abundant polychlorinated by-products were generated in the catalytic oxidation of CVOCs over the noble metals Pt and Pd [28,29]. V_2O_5/TiO_2 has been widely studied in the complete oxidation of chlorinated organic compounds, such as the

chlorobenzenes, chlorophenols, and polychlorinated biphenyl (PCBs), as well as polychlorinated dibenzo-p-dioxins and dibenzofurans (PCDD/Fs) [30–33]. Recently, much attention has been devoted to the transition metal oxides (Cr, Mn, Co, Fe), where catalyst deactivation was usually observed. Hence, it is still very meaningful to explore novel catalysts with the advantages of higher ability for anti-chlorine poisoning and less polychlorinated by-products.

Ruthenium-based catalysts have been well demonstrated in ammonia synthesis [34,35], CO oxidation [36–38], and the deacon reaction [39–43]. Under oxygen-rich conditions, a highly active RuO_2 layer was generated on the catalyst surface, and the oxidation reaction was highly promoted [44]. Sumitomo Chemical Corporation has built a demonstration plant for Cl_2 production through the deacon process over Ru-based catalysts, and the demo-plant has been running smoothly for two years, revealing that Ru catalysts exhibit excellent stability in chlorine-containing gas flow.

Recently, Ru-based catalysts have gained increasing importance in VOC oxidation, including ethyl acetate [45], propane [46–48], benzene [49], chlorobenzene [50,51], trichloroethylene [33,52], methyl bromide [53], and others. It is noteworthy that Ru catalysts contributed apparently higher catalytic activity than many reported catalysts with comparable loadings in CVOC oxidation [50,51,54].

Among the Ru-based catalysts, Ru/TiO_2 was recognized as the most promising catalyst in chlorine-containing oxidation reactions, such as the deacon reaction and CVOC oxidation. The supports commonly include the anatase, rutile, and P25 (mixed phase) TiO_2. P25 and rutile have been recognized as the most promising supports due to the strong interactions between rutile TiO_2 and RuO_2 due to their similar lattice spacing. Our group studied the oxidation of trichloroethylene over Ru/TiO_2 (anatase, rutile, and P25), and concluded that Ru/TiO_2-P25 contributed the highest catalytic activity and stability [33].

Bimetallic catalysts commonly show higher catalytic activity, selectivity, and anti-poisoning ability than monometallic materials due to the synergistic effect [49,55–62]. Yashnik et al. prepared Pd-Mn catalysts employed in methane oxidation, and a Pd-Mn synergistic effect was observed. Recently, CeO_2 has been widely studied due to its unique properties of high oxygen mobility and oxidative ability. Hence, it is of great interest to study the bimetallic catalysts $Ru\text{-}Ce/TiO_2$ (anatase, rutile, and P25) for CVOC oxidation.

Herein, a series of Ru-based mono- and bimetallic materials were prepared and evaluated in the catalytic oxidation of chlorobenzene. XRD, XPS, TEM, HAADF-STEM and H_2-TPR characterizations were conducted. Catalytic activities were well correlated with observed physicochemical properties.

2. Results and Discussion

2.1. Catalytic Oxidation of Chlorobenzene

The catalytic oxidation of chlorobenzene was conducted over different Ru-based samples, such as $1Ru/TiO_2$(P25), $1Ru/ZrO_2$, $1Ru/\gamma\text{-}Al_2O_3$, and $1Ru/SiO_2$. The results are summarized in Figure 1a. Among those catalysts, $1Ru/TiO_2$(P25) contributed the lowest complete oxidation temperature at 280 °C, revealing that commercial P25 TiO_2 was the best support for Ru catalysts in chlorobenzene oxidation, and it was believed that the rutile phase played an important role in the P25 support due to the similar interplanar lattice spacings for RuO_2 and rutile (110) of TiO_2. Besides, the intrinsic physicochemical properties of the supports are also of great concern on their catalytic performance. Considering that P25 exists as a mixed phase containing the anatase and rutile phases, $1Ru/TiO_2$(P25), $1Ru/TiO_2$(Anatase), and $1Ru/TiO_2$(Rutile) were prepared and compared in chlorobenzene oxidation. As shown in Figure 1b, $1Ru/TiO_2$(P25) was still the most active catalyst. $1Ru/TiO_2$(Rutile) gave far lower catalytic activity than the other two samples, and its conversion was below 50% at 350 °C. Similar phenomenon has been reported in our previous work on the catalytic oxidation of trichloroethylene over Ru/TiO_2 catalysts [33]. RuO_2 was commonly well-dispersed on rutile TiO_2, whereas RuO_2 sintering occurred on Ru/TiO_2(P25) and Ru/TiO_2(Anatase). However, particle size effect was often observed for noble metal catalysts. In this catalytic system, Ru/TiO_2(P25) showed

the highest activity than Ru/TiO_2(Rutile) and Ru/TiO_2(Anatase) according to the combined effects of dispersity and particle size effect.

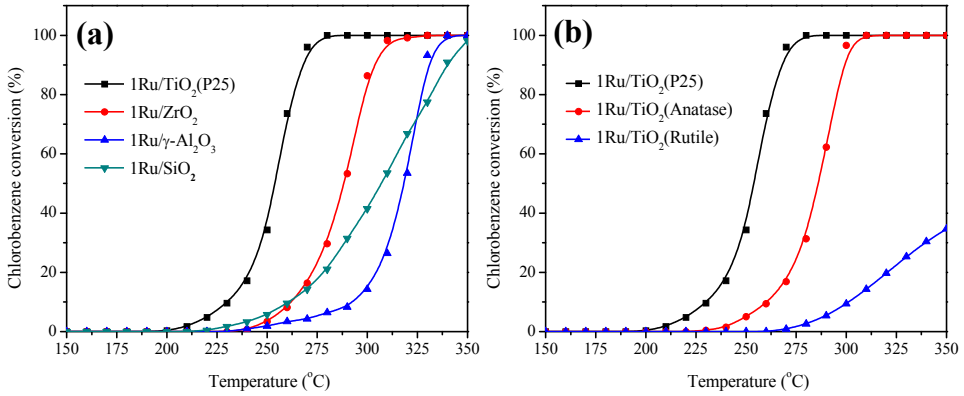

Figure 1. Chlorobenzene conversion as a function of reaction temperature over (**a**) $1Ru/TiO_2$(P25), $1Ru/ZrO_2$, $1Ru/\gamma$-Al_2O_3, and $1Ru/SiO_2$, and (**b**) $1Ru/TiO_2$(P25), $1Ru/TiO_2$(Anatase), and $1Ru/TiO_2$(Rutile) under the conditions of chlorobenzene concentration = 500 ppm, chlorobenzene/O_2 molar ratio = 1/400, and weight hourly space velocity (WHSV) = 60,000 mL/(g h).

Bimetallic catalysts commonly showed higher activity than monometallic catalysts due to the synergistic effect. To further increase in the catalytic activity of $1Ru/TiO_2$ materials, ceria oxides were introduced into the Ru catalytic system (Figure 2). The T_{90} of $1Ru\text{-}5Ce/TiO_2$(Rutile), $1Ru\text{-}5Ce/TiO_2$(P25), and $1Ru\text{-}5Ce/TiO_2$(Anatase) were 279, 283, and 290 °C, respectively. Surprisingly, the catalytic activity of $1Ru\text{-}5Ce/TiO_2$(Rutile) was dramatically improved. However, the catalytic activity of P25 supported catalysts decreased with Ce addition. $1Ru\text{-}5Ce/TiO_2$(Anatase) showed slight catalytic improvement in comparison to $1Ru/TiO_2$(Anatase). It could be concluded that the support crystal phase plays an important role in Ru-catalyzed chlorobenzene oxidation, which is consistent with previous reports.

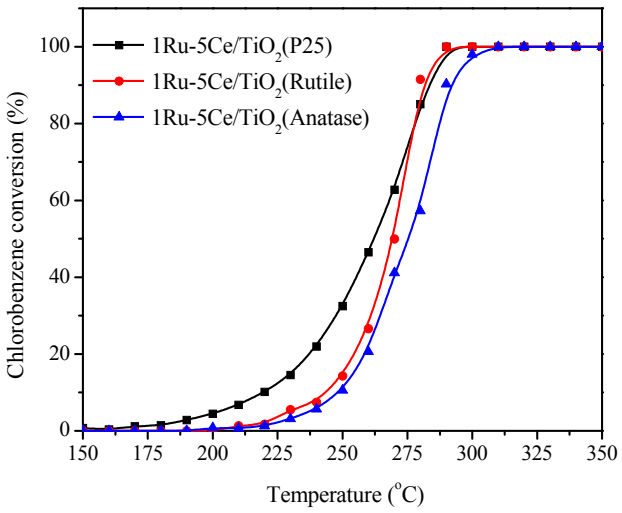

Figure 2. Chlorobenzene conversion as a function of reaction temperature over $1Ru\text{-}5Ce/TiO_2$ catalysts under the conditions of chlorobenzene concentration = 500 ppm, chlorobenzene/O_2 molar ratio = 1/400, and WHSV = 60,000 mL/(g h).

The chlorobenzene consumption rates for $1Ru/TiO_2$ and $1Ru\text{-}5Ce/TiO_2$ catalysts were compared at 280 °C (Figure 3). It is noteworthy that $1Ru/TiO_2$(P25) contributed the highest chlorobenzene

consumption rate (0.37 μmol/(g s)) as compared to the other samples, demonstrating that the monometallic Ru catalytic system was appropriate for P25 support. Obviously, 1Ru-5Ce/TiO_2(Rutile) gave a far higher chlorobenzene consumption rate (0.34 μmol/(g s)) than that of 1Ru/TiO_2(Rutile) (0.01 μmol/(g s)), revealing that the Ru-Ce bimetallic catalytic system was very suitable for rutile TiO_2 support. Considering the lower cost of rutile TiO_2 as compared to P25, it is very important to conduct systematic studies for rutile TiO_2 supported Ru-Ce bimetallic catalysts. It is noteworthy that Ru-5Ce/TiO_2(Rutile) showed comparable catalytic performance to Ru/TiO_2(P25), and the RuO_2 active species could be highly trapped and stabilized by TiO_2(Rutile) and CeO_2, which was proved in the HAADF-STEM images.

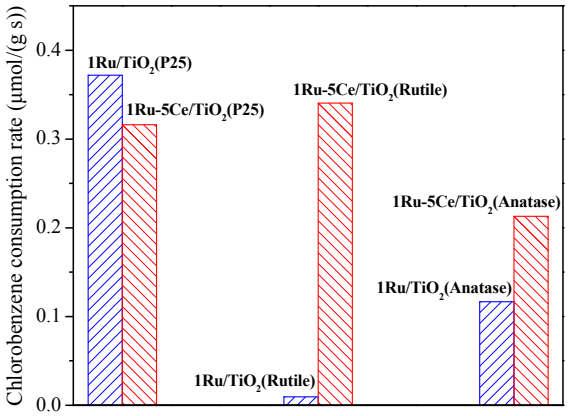

Figure 3. Chlorobenzene consumption rates for 1Ru/TiO_2 and 1Ru-5Ce/TiO_2 catalysts at 280 °C.

To evaluate catalytic stability, on-stream chlorobenzene oxidation experiments were carried out for 1Ru-5Ce/TiO_2(P25), 1Ru-5Ce/TiO_2(Rutile), and 1Ru-5Ce/TiO_2(Anatase). As shown in Figure 4a, 1Ru-5Ce/TiO_2(Rutile) gave best catalytic performance at 280 °C. For 1Ru-5Ce/TiO_2(Rutile) and 1Ru-5Ce/TiO_2(P25), the chlorobenzene conversion stabilized at approximately 91% and 86%, respectively. Although 1Ru-5Ce/TiO_2(Anatase) activity showed an increasing trend over time, its catalytic activity was far lower than other two materials. Besides, light-off curves with cycle experiments were conducted. As shown in Figure 4b, the catalytic activity slightly decreased within the fourth runs. However, the catalytic activity was then stabilized, and the conversion in 16th run was basically comparable to the 4th run, indicating excellent stability for 1Ru-5Ce/TiO_2(Rutile).

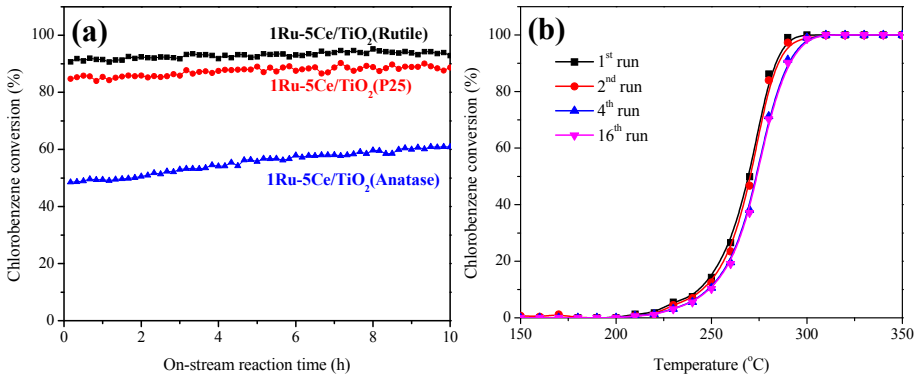

Figure 4. (**a**) Chlorobenzene conversion as a function of on-stream reaction time at 280 °C over the 1Ru-5Ce/TiO_2 catalysts; (**b**) cycle experiments over 1Ru-5Ce/TiO_2(Rutile) under the conditions of chlorobenzene concentration = 500 ppm, chlorobenzene/O_2 molar ratio = 1/400, and WHSV = 60,000 mL/(g h).

For VOCs purification applications, CO_2 selectivity was also an important factor for the catalyst. In the catalytic oxidation of chlorobenzene over 1Ru/TiO_2(Rutile) and 1Ru-5Ce/TiO_2(Rutile), organic byproducts such as multi-chlorinated benzenes were basically not observed. Hence, the CO_2 selectivity was calculated based on CO_2 and CO. As shown in Figure 5, 1Ru-5Ce/TiO_2(Rutile) gave excellent CO_2 selectivity (98–100%), which was apparently better than 1Ru/TiO_2(Rutile), revealing that Ru-Ce bimetallic catalytic system was beneficial to enhencing CO_2 selectivity.

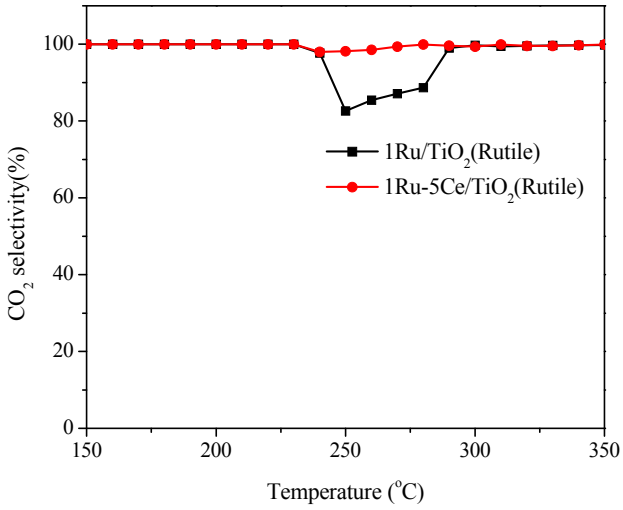

Figure 5. CO_2 selectivity of chlorobenzene oxidation over 1Ru/TiO_2(Rutile) and 1Ru-5Ce/TiO_2(Rutile) under the conditions of chlorobenzene concentration = 500 ppm, chlorobenzene/O_2 molar ratio = 1/400, and WHSV = 60,000 mL/(g h).

2.2. Catalyst Characterization

The XRD patterns of Ru-based monometallic and bimetallic catalysts were collected. As shown in Figure 6a, 1Ru/TiO_2(P25) and 1Ru/ZrO_2 showed no peaks ascribed to ruthenium species, possibly due to being well dispersed. For 1Ru/SiO_2 and 1Ru/γ-Al_2O_3, peaks attributable to RuO_2 were observed at 28.0°, 35.1°, and 54.3°, revealing that RuO_2 was easily aggregated on the SiO_2 and γ-Al_2O_3 surface, suggesting that this could be the main reason for their poor catalytic activities. In Figure 6b, 1Ru/TiO_2 and 1Ru-5Ce/TiO_2 showed similar XRD patterns, and no ceria species were observed.

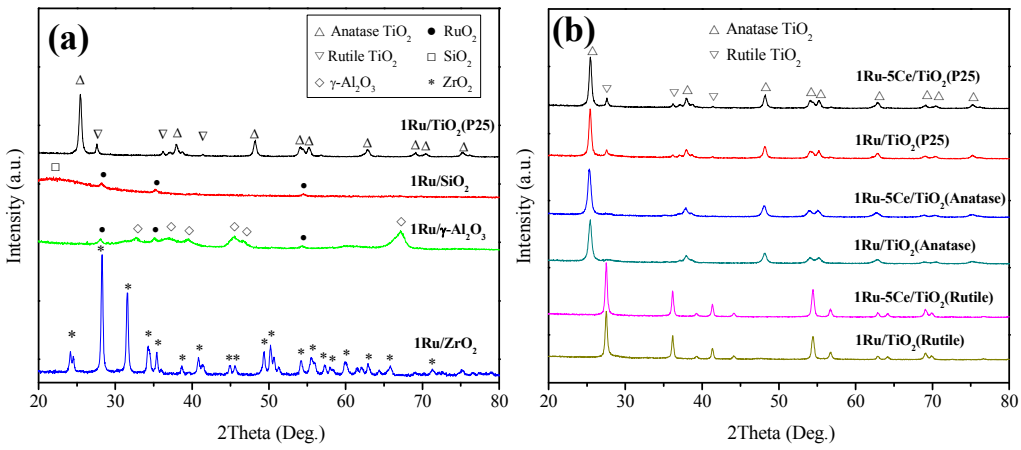

Figure 6. XRD patterns of (**a**) 1Ru/TiO_2(P25), 1Ru/ZrO_2, 1Ru/γ-Al_2O_3, and 1Ru/SiO_2, and (**b**) 1Ru/TiO_2 and 1Ru-5Ce/TiO_2.

XPS spectra for the catalysts 1Ru/TiO_2 and 1Ru-5Ce/TiO_2 were obtained; the Ru 3d and O 1s spectra are illustrated in Figure 7. As shown in Figure 7a, the supports of P25 and anatase gave the main peaks at similar a binding energy, whereas the rutile TiO_2 support showed a major peak at a higher binding energy (BE) value. The main peaks showed apparent shifts to the high BE value after the addition of the CeO_2. Considering that the assignments and definitions of Ru peaks were inconsistent in previous studies, and apparent shifts were observed, Ru 3d spectra were not de-convoluted in this research. The XPS data were summarized in Table 1. It could be seen that 1Ru/TiO_2(Rutile) contributed the highest Ru content on the catalyst surface, whereas giving the lowest catalytic activity, revealing that the dispersion was not the only factor influencing the catalytic performance. As illustrated in Figure 7b, O 1s were de-convoluted into two peaks at 529.8 and 531.8 eV, ascribed to O_{latt} (lattice oxygen) and O_{ads} (adsorbed oxygen, e.g., O_2^-, O_2^{2-}, or O^-), respectively. It was generally believed that the electrophilic O_{ads} species play an important role in VOCs oxidation. For the three 1Ru-5Ce/TiO_2 catalysts, 1Ru-5Ce/TiO_2(Rutile) contributed the highest Ru/Ce ratio (0.3) and O_{ads} /O_{latt} ratio (0.2) possibly due to the synergistic effect between Ru and Ce.

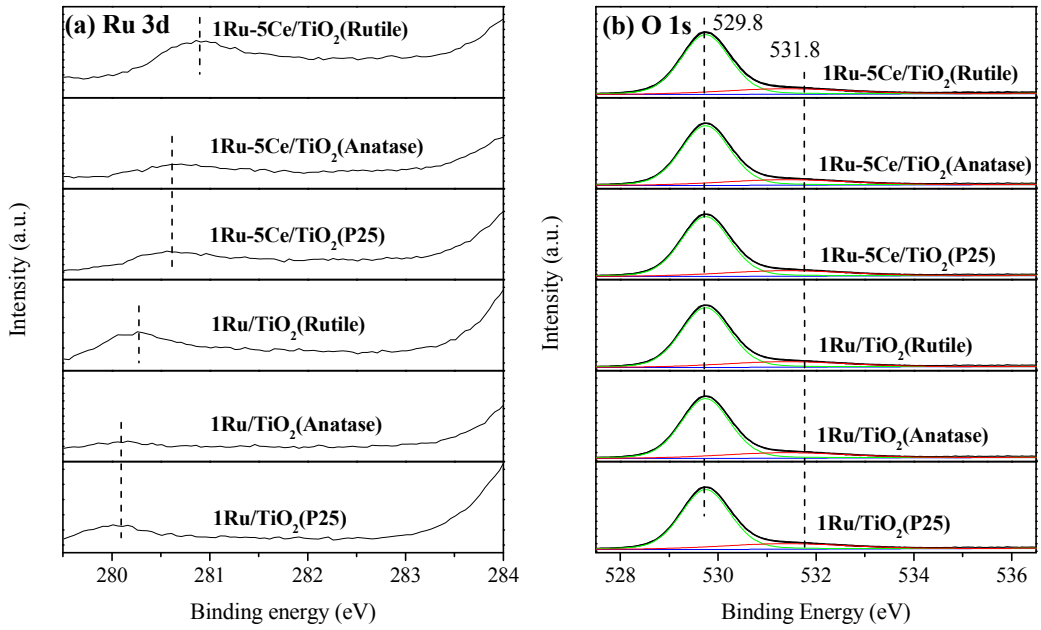

Figure 7. XPS spectra of Ru 3d (**a**) and O 1s (**b**) for Ru-based catalysts.

Table 1. XPS data of 1Ru/TiO_2 and 1Ru-5Ce/TiO_2.

Catalysts	Ru (at. %)	Ce (at. %)	Ru/Ce	O_{ads}/O_{latt}
1Ru/TiO_2(P25)	0.5	-	-	0.2
1Ru/TiO_2(Anatase)	0.2	-	-	0.1
1Ru/TiO_2(Rutile)	0.7	-	-	0.2
1Ru-5Ce/TiO_2(P25)	0.5	2.6	0.2	0.2
1Ru-5Ce/TiO_2(Anatase)	0.3	1.9	0.1	0.2
1Ru-5Ce/TiO_2(Rutile)	0.7	3.4	0.3	0.2

TEM and high resolution transmission electron microscopy (HRTEM) characterizations were conducted to identify the morphology of 1Ru/TiO_2(Rutile) and 1Ru-5Ce/TiO_2(Rutile). As shown in Figure 8a,b, RuO_2 species were not observed on the surface of 1Ru/TiO_2(Rutile), possibly due to its thin layer structure which usually showed a low contrast in TEM images. However, for 1Ru-5Ce/TiO_2(Rutile), abundant RuO_2 nanoparticles were observed (Figure 8c), revealing that RuO_2 nanoparticles were easily formed in the presence of CeO_2. Interplanar lattice spacings for RuO_2 and

rutile (110) of TiO_2 were observed, and it could be seen that they exhibit similar lattice spacing values. Hence, RuO_2 nanoparticles could be highly stabilized by TiO_2(Rutile), leading to higher catalytic activity and stability than other bimetallic materials.

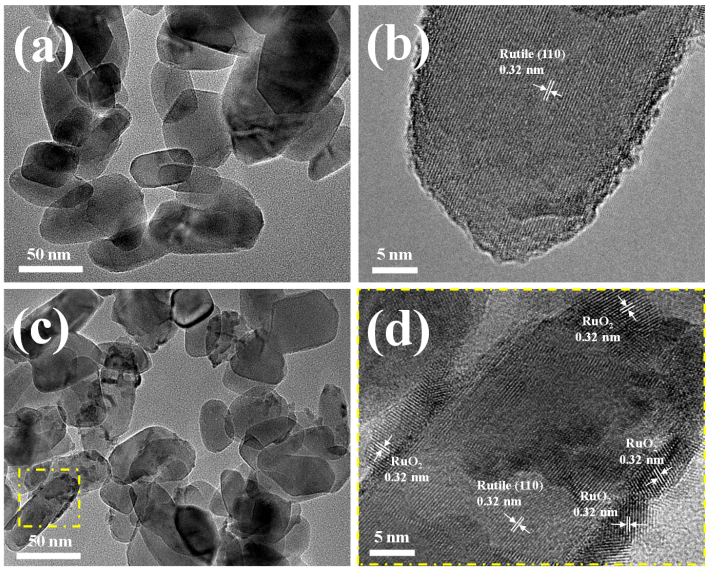

Figure 8. TEM and HRTEM images of the catalysts: (**a**,**b**) 1Ru/TiO_2(Rutile), and (**c**,**d**) 1Ru-5Ce/TiO_2(Rutile).

To further explore the distributions of monometallic Ru and bimetallic Ru-Ce species, HAADF-STEM and STEM-energy dispersive X-ray spectroscopy (STEM-EDS) mapping images were collected for 1Ru/TiO_2(Rutile) and 1Ru-5Ce/TiO_2(Rutile). As shown in Figure 9, the distributions for Ru (green), Ti (red), and Ce (purple) are presented. For 1Ru/TiO_2(Rutile), Ru and Ti showed a similar distribution, indicating that RuO_2 was highly dispersed on the rutile TiO_2 support due to their similar crystal lattice spacing values. However, the highly dispersed catalyst gave poor catalytic performance, revealing that dispersion was not the major factor for the catalytic activity, which was different from the other catalytic systems. For 1Ru-5Ce/TiO_2(Rutile), it was interestingly observed that Ru species were surrounded by CeO_2 and therefore forming the trapped RuO_2. In consideration of its high activity, it was proposed that this unique structure greatly facilitated catalytic activity and stability.

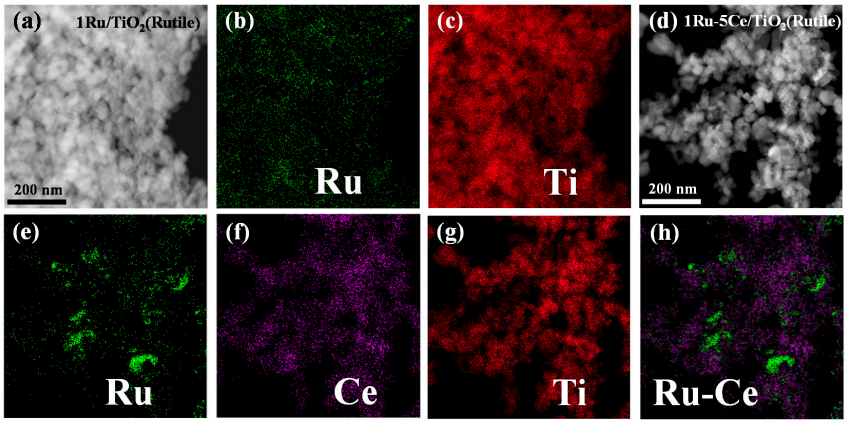

Figure 9. Representative HAADF-STEM images (**a**,**d**) and STEM-EDS mapping images of (**b**,**e**) Ru, (**e**,**g**) Ti, and (**f**) Ce, and (**h**) Ru-Ce for 1Ru/TiO_2(Rutile) (**a**–**c**) and 1Ru-5Ce/TiO_2(Rutile) (**d**–**h**).

In order to research the reducibility of the catalysts, H_2-TPR profiles of 1Ru-5Ce/TiO_2(Rutile), 1Ru/TiO_2(Rutile), and 5Ce/TiO_2(Rutile) were collected and summarized in Figure 10. A single reduction peak at 150 °C for 1Ru/TiO_2(Rutile), which was ascribed to the reduction of RuO_2 to metallic Ru, and the actual H_2 consumption was 0.187 mmol/g, which was close to the theoretical value (0.198 mmol/g) calculated by assuming that all Ru atoms in the catalysts existed as Ru^{4+}. For 1Ru-5Ce/TiO_2(Rutile), a broad peak at 128 °C was observed assigned to the overlapping of the reduction of RuO_2 and the active oxygen species in CeO_2. Apparently, the reducibility was enhanced in the Ru-Ce bimetallic catalyst, suggesting a synergistic effect between Ru and Ce in 1Ru-5Ce/TiO_2(Rutile). The hydrogen spillover effect was commonly observed in the low temperature reduction of a catalyst composed of transition metal oxide and noble metal [49].

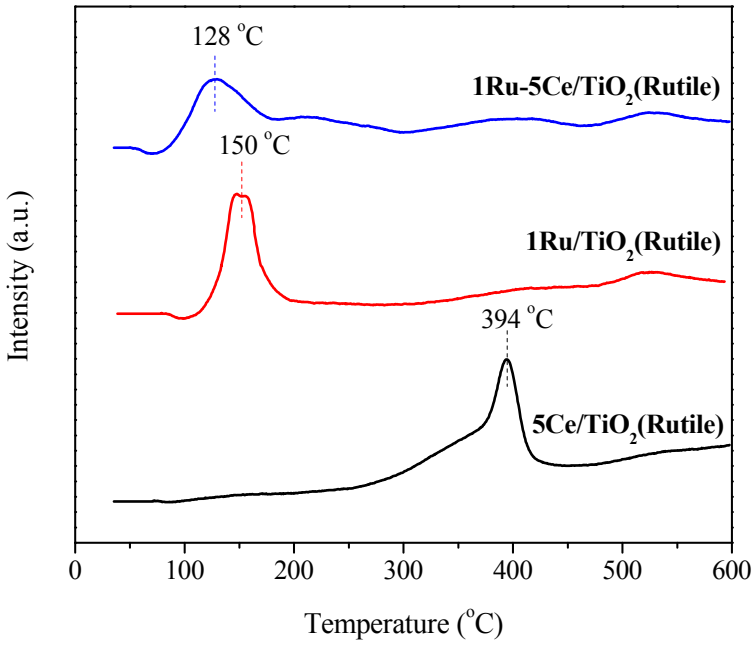

Figure 10. H_2-TPR profiles of 1Ru-5Ce/TiO_2(Rutile), 1Ru/TiO_2(Rutile), and 5Ce/TiO_2(Rutile).

2.3. In Situ FTIR Studies and Reaction Mechanism

To further investigate the reaction mechanism of chlorobenzene oxidation over 1Ru-5Ce/TiO_2(Rutile), in situ FTIR spectra were collected. As shown in Figure 11, the band at 1892 cm^{-1} was tentatively ascribed to the trace maleic anhydride coordinated to $Ru^{\delta+}$ at the corner sites of the RuO_x clusters according to the previous research [49]. The band at 1598 cm^{-1} was ascribed to the phenolate species. The band at 1731 cm^{-1} was assigned to the C=O from quinone or other ketone species [23]. The bands between 1568–1526 cm^{-1} were due to the COO-antisymmetric stretching vibration of (chlorinated)-maleate and acetates, and the band at 1404 cm^{-1} was attributable to the COO-symmetric stretching vibrations of (chlorinated)-maleate and acetates. The band at 1367 cm^{-1} was assigned to the –CH_2–stretching vibration of (chlorinated)-acetates.

Accordingly, the reaction mechanism was proposed. As shown in Figure 12, in comparison to 1Ru/TiO_2(Rutile), 1Ru-5Ce/TiO_2(Rutile) contributed a much higher catalytic efficiency due to its trapped RuO_2 structure caused by CeO_2. During the oxidation, CeO_2 also play an important role for affording the active oxygen species, which facilitated the oxidation of chlorobenzene over RuO_2 centers. For 1Ru-5Ce/TiO_2(Rutile) (A), chlorobenzene (B) was firstly oxidized into phenolate species (C). Then, the phenolate species are further oxidized into o-benzoquinone (D) and p-benzoquinone (E). Subsequently, small organic intermediates are generated through the ring-opening process, and the intermediates are easily chlorinated by the chlorine released from catalyst surface (C), leading to

(chlorinated)-maleate (F) and acetates (G). Finally, the intermediates are decomposed into CO_2, H_2O, HCl, and Cl_2.

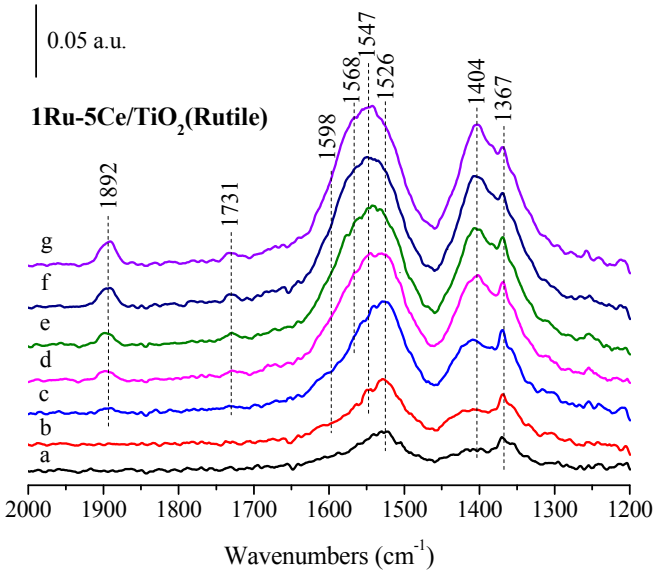

Figure 11. In situ FTIR spectra for 1Ru-5Ce/TiO_2(Rutile) collected at 290 °C after (a) 1; (b) 3; (c) 10; (d) 20; (e) 30; (f) 60; (g) 90 min on 500 ppm benzene/Ar stream.

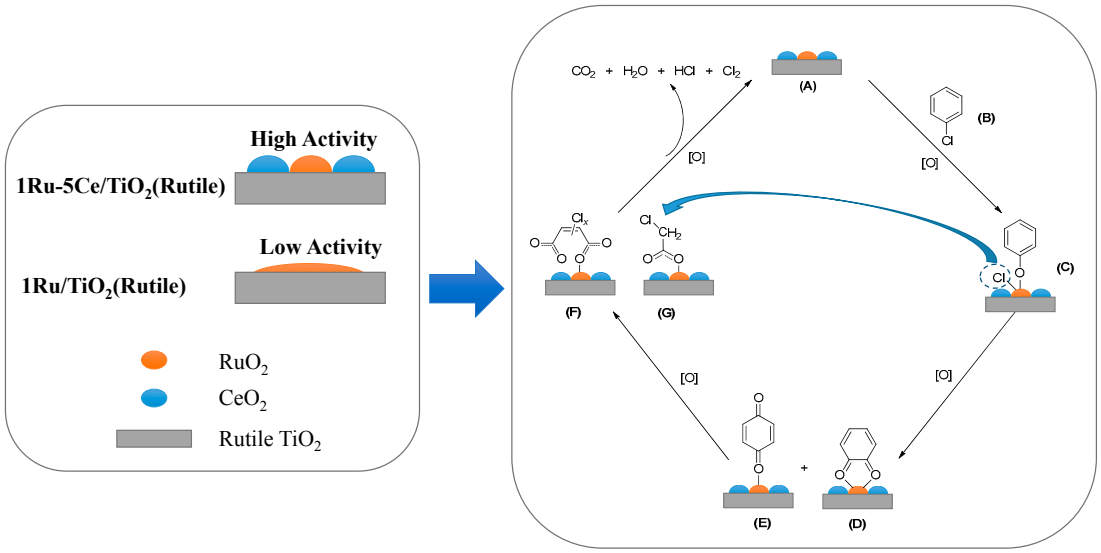

Figure 12. The reaction mechanism of chlorobenzene oxidation over 1Ru-5Ce/TiO_2(Rutile).

3. Materials and Methods

3.1. Catalyst Preparation

1Ru/Support samples were prepared using an impregnation method with 1 wt % Ru. In a standard preparation of 1Ru/TiO_2-P25, commercial P25 TiO_2 (Degussa, Essen, Germany) was mixed with an aqueous solution of $Ru(NO)(NO_3)_3$ (1.5 mg/mL, Aladdin, Shanghai, China). The mixture was stirred for 5 h at room temperature. Then, the solvent was removed under vacuum, and the solid was dried at 110 °C for 5 h. Subsequently, the resulting solid was calcined at 350 °C for 4 h, giving the final product of 1Ru/TiO_2(P25). The samples of 1Ru/SiO_2, 1Ru/γ-Al_2O_3, 1Ru/TiO_2(Anatase),

and 1Ru/TiO_2(Rutile) were prepared using the same method by changing the supports (SiO_2, γ-Al_2O_3, TiO_2(Anatase), and TiO_2(Rutile) were purchased from Aladdin, Shanghai, China).

The 1Ru-5Ce/TiO_2 catalysts were prepared through a step-impregnation method. The percentage of elemental Ru was 1 wt % and that of CeO_2 was 5 wt %. In a standard preparation of 1Ru-5Ce/TiO_2-P25, commercial P25 TiO_2 (Degussa, Essen, Germany) was mixed with the solution of $Ce(NO_3)_3$ $6H_2O$ (Aladdin, Shanghai, China), and the solid was dried at 110 °C for 5 h. Subsequently, the resulting solid was calcined at 350 °C for 4 h, giving 5Ce/TiO_2-P25. Subsequently, an aqueous solution of $Ru(NO)(NO_3)_3$ (1.5 mg/mL, Aladdin, Shanghai, China) was mixed with the suspension of 5Ce/TiO_2, and the mixture was stirred for 5 h at room temperature. Then, the solvent was removed under vacuum, and the resulting solid was dried at 110 °C for 5 h. Finally, the solid was calcined at 350 °C for 4 h, giving the final product of 1Ru-5Ce/TiO_2-P25.

3.2. Catalyst Characterization

The catalysts were characterized using various techniques. X-ray diffraction (XRD) patterns of the catalysts were collected with a powder diffractometer (Rigaku D/Max-RA, Rigaku, Tokyo, Japan) using Cu Kα radiation (40 kV and 120 mA). The surface area and pore diameter were characterized by N_2 adsorption at 77 K in an automatic surface area and porosity analyzer (Autosorb iQ, Quantachrome, Boynton Beach, FL, USA). Transmission electron microscopy (TEM), high resolution transmission electron microscopy (HR-TEM), and high-angle, annular, dark-field scanning TEM (HAADF-STEM) images were recorded on an FEI Tecnai G^2 F20 field emission electron microscope (FEI, Hillsboro, OR, USA) operating at 200 kV. X-ray photoelectron spectroscopy (XPS) analyses were performed with a Thermo Scientific ESCALAB 250Xi (Thermo Fisher Scientific, Waltham, MA, USA) X-ray using an Al Kα source. Hydrogen temperature programmed reduction (H_2-TPR) was carried out on an AutoChemII 2920 apparatus (Micromeritics, Atlanta, GA, USA) with a flow-type reactor. FTIR spectra were collected using an FTIR spectrometer (Nicolet 6700, Thermo Fisher Scientific, Waltham, MA, USA) equipped with an MCT detector (cooled by liquid nitrogen) and a stainless steel IR cell (CaF_2 windows).

3.3. Catalytic Evaluation

The catalysts were evaluated in a fixed-bed, quartz micro-reactor (i.d. = 4 mm) from 100 to 350 °C with 100 mg of catalyst (60–80 mesh). In the middle of the quartz microreactor, a quartz sieve was fixed, and the catalyst was placed on the quartz sieve. Chlorobenzene was introduced from a gas cylinder, and its concentration, as part of the total flow (500 ppm Chlorobenzene + 20% O_2 + Ar (balance)), was calibrated by a gas chromatography (GC 2010 Plus, Shimadzu, Kyoto, Japan) using a bypass. The total flow ratio of the reactant mixture was 100 mL/min, and the weight hourly space velocity (WHSV) was 60,000 mL/(g h). The reactants and products were analyzed on-line with a gas chromatography (GC 2010 Plus, Shimadzu, Kyoto, Japan) equipped with a flame ionization detector (FID). The conversion of chlorobenzene was calculated using Equation (1).

$$X = \frac{[\mathrm{C(in)} - \mathrm{C(out)}]}{\mathrm{C(in)}} \times 100\%, \quad (1)$$

where X is the conversion, and C(in) and C(out) are the inlet and outlet concentrations of chlorobenzene, respectively. The reactants and products (CO_2 and CO) were analyzed on-line with a gas chromatography (GC 2010 Plus, Shimadzu, Kyoto, Japan) equipped with a methanizer (MTH, Shimadzu, Kyoto, Japan) furnace and two flame ionization detectors (FID). In the catalytic oxidation of chlorobenzene, organic byproducts were not observed by GC. Hence, the CO_2 selectivity was calculated using the equation: CO_2 selectivity = [$C(CO_2)$/($C(CO_2)$ + C(CO))].

4. Conclusions

Among the different Ru-based catalysts, 1Ru/TiO_2(P25) showed the greatest activity in chlorobenzene oxidation, revealing that commercial P25 TiO_2 was the best support for Ru catalysts. After ceria oxides were introduced into the Ru catalytic system, the T_{90} of 1Ru-5Ce/TiO_2(Rutile), 1Ru-5Ce/TiO_2(P25), and 1Ru-5Ce/TiO_2(Anatase) were 279, 283, and 290 °C, respectively, revealing that the support crystal phase plays an important role in Ru-catalyzed chlorobenzene oxidation. Comparing the consumption rates for the 1Ru/TiO_2 and 1Ru-5Ce/TiO_2 catalysts, it can be concluded that the optimum support for each catalytic system was different. For 1Ru-5Ce/TiO_2(P25), 1Ru-5Ce/TiO_2(Rutile), and 1Ru-5Ce/TiO_2(Anatase), and 1Ru-5Ce/TiO_2(Rutile) gave the best catalytic performance at 280 °C; the chlorobenzene conversion of 1Ru-5Ce/TiO_2(Rutile) and 1Ru-5Ce/TiO_2(P25) were found to be approximately 91% and 86%, respectively. According to XRD patterns, it can be concluded that the poor catalytic activities of Ru/SiO_2 and 1Ru/γ-Al_2O_3 were due to RuO_2 easily aggregating on the supports. According to the XPS spectra, it is believed that the electrophilic O_{ads} species play an important role in VOCs oxidation. Compared to the 1Ru/TiO_2(Rutile), abundant RuO_2 nanoparticles were observed on the surface of 1Ru-5Ce/TiO_2(Rutile), thereby leading to higher catalytic activity and stability. According to the HAADF-STEM and STEM-EDS mapping images, dispersion was not the major factor for the catalytic activity; the unique structure greatly facilitated the catalytic activity and stability. Compared with 1Ru/TiO_2(Rutile), 1Ru-5Ce/TiO_2(Rutile) contributed a much higher catalytic efficiency because of its trapped RuO_2 structure, caused by CeO_2. Additionally, the reaction mechanism was proposed according to the intermediates observed in the in situ FTIR studies.

Acknowledgments: This work was supported by Natural Science Foundation of China (21607154).

Author Contributions: Meng Ye and Tingyu Zhu conceived and designed the experiments; Meng Ye, Li Chen, Xiaolong Liu, Wenqing Xu, and Guanyi Chen performed the experiments; Meng Ye and Tingyu Zhu analyzed the data; and Meng Ye wrote the paper.

Conflicts of Interest: The authors declare no conflicts of interest. The founding sponsors had no role in the design of the study; the collection, analyses, or interpretation of data; the writing of the manuscript; or the decision to publish the results.

References

1. Jiang, L.; Nie, G.; Zhu, R.; Wang, J.; Chen, J.; Mao, Y.; Cheng, Z.; Anderson, W.A. Efficient degradation of chlorobenzene in a non-thermal plasma catalytic reactor supported on CeO_2/HZSM-5 catalysts. *J. Environ. Sci.* **2017**, *55*, 266–273. [CrossRef] [PubMed]
2. Zhang, X.; Xue, Z.; Hong, L.; Li, Y.; Yuan, Y.; Yi, W.; Duan, J.; Lei, L.; Chai, F.; Cheng, M. Ambient volatile organic compounds pollution in China. *J. Environ. Sci.* **2017**, *55*, 69–75. [CrossRef] [PubMed]
3. Liu, B.; Li, X.; Zhao, Q.; Liu, J.; Liu, S.; Wang, S.; Tade, M.O. Insight into the Mechanism of Photocatalytic Degradation of Gaseous o-dichlorobenzene over Flower-Type V_2O_5 Hollow Spheres. *J. Mater. Chem. A* **2015**, *3*, 15163–15170. [CrossRef]
4. Huang, B.; Lei, C.; Wei, C.; Zeng, G. Chlorinated volatile organic compounds (Cl-VOCs) in environment—Sources, potential human health impacts, and current remediation technologies. *Environ. Int.* **2014**, *71*, 118–138. [CrossRef] [PubMed]
5. Delaigle, R.; Debecker, D.P.; Bertinchamps, F.; Gaigneaux, E.M. Revisiting the behaviour of vanadia-based catalysts in the abatement of (chloro)-aromatic pollutants: Towards an integrated understanding. *Top. Catal.* **2009**, *52*, 501. [CrossRef]
6. Gan, J.; Megonnell, N.E.; Yates, S.R. Adsorption and catalytic decomposition of methyl bromide and methyl iodide on activated carbons. *Atmos. Environ.* **2001**, *35*, 941–947. [CrossRef]
7. Everaert, K.; Baeyens, J. Catalytic combustion of volatile organic compounds. *J. Hazard. Mater.* **2004**, *109*, 113–139. [CrossRef] [PubMed]
8. Li, J.; Lu, R.; Dou, B.; Ma, C.; Hu, Q.; Liang, Y.; Wu, F.; Qiao, S.; Hao, Z. Porous graphitized carbon for adsorptive removal of benzene and the electrothermal regeneration. *Environ. Sci. Technol.* **2012**, *46*, 12648–12654. [CrossRef] [PubMed]

9. Fiorenza, R.; Bellardita, M.; Palmisano, L.; Scirè, S. A comparison between photocatalytic and catalytic oxidation of 2-Propanol over Au/TiO_2-CeO_2 catalysts. *J. Mol. Catal. A Chem.* **2016**, *415*, 56–64. [CrossRef]
10. Hetrick, C.E.; Patcas, F.; Amiridis, M.D. Effect of water on the oxidation of dichlorobenzene over V_2O_5/TiO_2 catalysts. *Appl. Catal. B Environ.* **2011**, *101*, 622–628. [CrossRef]
11. Ojala, S.; Pitkäaho, S.; Laitinen, T.; Koivikko, N.N.; Brahmi, R.; Gaálová, J.; Matejova, L.; Kucherov, A.; Päivärinta, S.; Hirschmann, C. Catalysis in VOC abatement. *Top. Catal.* **2011**, *54*, 1224. [CrossRef]
12. Huang, H.; Xu, Y.; Feng, Q.; Leung, D.Y. Low temperature catalytic oxidation of volatile organic compounds: A review. *Catal. Sci. Technol.* **2015**, *5*, 2649–2669. [CrossRef]
13. Pitkäaho, S.; Nevanperä, T.; Matejova, L.; Ojala, S.; Keiski, R.L. Oxidation of dichloromethane over Pt, Pd, Rh, and V_2O_5 catalysts supported on Al_2O_3, Al_2O_3-TiO_2 and Al_2O_3-CeO_2. *Appl. Catal. B Environ.* **2013**, *138*, 33–42. [CrossRef]
14. Matějová, L.; Topka, P.; Kaluža, L.; Pitkäaho, S.; Ojala, S.; Gaálová, J.; Keiski, R.L. Total oxidation of dichloromethane and ethanol over ceria-zirconia mixed oxide supported platinum and gold catalysts. *Appl. Catal. B Environ.* **2013**, *142*, 54–64. [CrossRef]
15. Scirè, S.; Liotta, L.F. Supported gold catalysts for the total oxidation of volatile organic compounds. *Appl. Catal. B Environ.* **2012**, *125*, 222–246. [CrossRef]
16. López-Fonseca, R.; Gutiérrez-Ortiz, J.I.; Gutiérrez-Ortiz, M.A.; González-Velasco, J.R. Catalytic oxidation of aliphatic chlorinated volatile organic compounds over Pt/H-BETA zeolite catalyst under dry and humid conditions. *Catal. Today* **2005**, *107*, 200–207. [CrossRef]
17. González-Velasco, J.; Aranzabal, A.; Gutiérrez-Ortiz, J.; López-Fonseca, R.; Gutiérrez-Ortiz, M. Activity and product distribution of alumina supported platinum and palladium catalysts in the gas-phase oxidative decomposition of chlorinated hydrocarbons. *Appl. Catal. B Environ.* **1998**, *19*, 189–197. [CrossRef]
18. Khaleel, A.; Nawaz, M. Enhanced catalytic complete oxidation of 1,2-dichloroethane over mesoporous transition metal-doped γ-Al_2O_3. *J. Environ. Sci.* **2015**, *29*, 199–209. [CrossRef] [PubMed]
19. Durán, F.G.; Barbero, B.P.; Cadús, L.E.; Rojas, C.; Centeno, M.A.; Odriozola, J.A. Manganese and iron oxides as combustion catalysts of volatile organic compounds. *Appl. Catal. B Environ.* **2009**, *92*, 194–201. [CrossRef]
20. Garcia, T.; Sellick, D.; Varela, F.; Vázquez, I.; Dejoz, A.; Agouram, S.; Taylor, S.H.; Solsona, B. Total oxidation of naphthalene using bulk manganese oxide catalysts. *Appl. Catal. A Gen.* **2013**, *450*, 169–177. [CrossRef]
21. Liotta, L.F.; Wu, H.; Pantaleo, G.; Venezia, A.M. ChemInform Abstract: Co_3O_4 Nanocrystals and Co_3O_4—MO_x Binary Oxides for CO, CH_4 and VOC Oxidation at Low Temperatures: A Review. *Cheminform* **2014**, *45*, 3085–3102. [CrossRef]
22. Solsona, B.; García, T.; Sanchis, R.; Soriano, M.D.; Moreno, M.; Rodríguez-Castellón, E.; Agouram, S.; Dejoz, A.; Nieto, J.M.L. Total oxidation of VOCs on mesoporous iron oxide catalysts: Soft chemistry route versus hard template method. *Chem. Eng. J.* **2016**, *290*, 273–281. [CrossRef]
23. Wang, J.; Wang, X.; Liu, X.; Zhu, T.; Guo, Y.; Hao, Q. Catalytic oxidation of chlorinated benzenes over V_2O_5/TiO_2 catalysts: The effects of chlorine substituents. *Catal. Today* **2015**, *241*, 92–99. [CrossRef]
24. Tseng, T.K.; Wang, L.; Ho, C.T.; Chu, H. The destruction of dichloroethane over a γ-alumina supported manganese oxide catalyst. *J. Hazard. Mater.* **2010**, *178*, 1035–1040. [CrossRef] [PubMed]
25. Debecker, D.P.; Delaigle, R.; Bouchmella, K.; Eloy, P.; Gaigneaux, E.M.; Mutin, P.H. Total oxidation of benzene and chlorobenzene with MoO_3- and WO_3-promoted V_2O_5/TiO_2 catalysts prepared by a nonhydrolytic sol-gel route. *Catal. Today* **2010**, *157*, 125–130. [CrossRef]
26. Bertinchamps, F.; Poleunis, C.; Grégoire, C.; Eloy, P.; Bertrand, P.; Gaigneaux, E.M. Elucidation of deactivation or resistance mechanisms of CrO_x, VO_x and MnO_x supported phases in the total oxidation of chlorobenzene via ToF-SIMS and XPS analyses. *Surf. Interface Anal.* **2010**, *40*, 231–236. [CrossRef]
27. Abdullah, A.Z.; Bakar, M.Z.; Bhatia, S. Combustion of chlorinated volatile organic compounds (VOCs) using bimetallic chromium-copper supported on modified H-ZSM-5 catalyst. *J. Hazard. Mater.* **2006**, *129*, 39–49. [CrossRef] [PubMed]
28. Liotta, L.F. Catalytic oxidation of volatile organic compounds on supported noble metals. *Appl. Catal. B Environ.* **2010**, *100*, 403–412. [CrossRef]
29. Brink, R.W.V.D.; Louw, R.; Mulder, P. Formation of polychlorinated benzenes during the catalytic combustion of chlorobenzene using a Pt/γ-Al_2O_3 catalyst. *Appl. Catal. B Environ.* **1998**, *16*, 219–226. [CrossRef]
30. Huang, H.; Dai, Q.; Wang, X. Morphology effect of Ru/CeO_2 catalysts for the catalytic combustion of chlorobenzene. *Appl. Catal. B Environ.* **2014**, *158*, 96–105. [CrossRef]

31. Hetrick, C.E.; Lichtenberger, J.; Amiridis, M.D. Catalytic oxidation of chlorophenol over V_2O_5/TiO_2 catalysts. *Appl. Catal. B Environ.* **2008**, *77*, 255–263. [CrossRef]
32. Bertinchamps, F.; Grégoire, C.; Gaigneaux, E.M. Systematic investigation of supported transition metal oxide based formulations for the catalytic oxidative elimination of (chloro)-aromatics: Part II: Influence of the nature and addition protocol of secondary phases to VO_x/TiO_2. *Appl. Catal. B Environ.* **2006**, *66*, 10–22. [CrossRef]
33. Wang, J.; Liu, X.; Zeng, J.; Zhu, T. Catalytic oxidation of trichloroethylene over TiO_2 supported ruthenium catalysts. *Catal. Commun.* **2016**, *76*, 13–18. [CrossRef]
34. Raróg-Pilecka, W.; Miśkiewicz, E.; Szmigiel, D.; Kowalczyk, Z. Structure sensitivity of ammonia synthesis over promoted ruthenium catalysts supported on graphitised carbon. *J. Catal.* **2005**, *231*, 11–19. [CrossRef]
35. Siporin, S.E.; Davis, R.J. Use of kinetic models to explore the role of base promoters on Ru/MgO ammonia synthesis catalysts. *J. Catal.* **2004**, *225*, 359–368. [CrossRef]
36. Öström, H.; Öberg, H.; Xin, H.; Larue, J.; Beye, M.; Dell'Angela, M.; Gladh, J.; Ng, M.L.; Sellberg, J.A.; Kaya, S. Surface chemistry. Probing the transition state region in catalytic CO oxidation on Ru. *Science* **2015**, *347*, 978–982. [CrossRef] [PubMed]
37. Qadir, K.; Sang, H.J.; Mun, B.S.; Butcher, D.R.; Renzas, J.R.; Aksoy, F.; Zhi, L.; Somorjai, G.A.; Park, J.Y. Intrinsic Relation between Catalytic Activity of CO Oxidation on Ru Nanoparticles and Ru Oxides Uncovered with Ambient Pressure XPS. *Nano Lett.* **2012**, *12*, 5761–5768. [CrossRef] [PubMed]
38. Gao, F.; Goodman, D.W. CO oxidation over ruthenium: Identification of the catalytically active phases at near-atmospheric pressures. *Phys. Chem. Chem. Phys.* **2012**, *14*, 6688–6697. [CrossRef] [PubMed]
39. Crihan, D.; Knapp, M.; Zweidinger, S.; Lundgren, E.; Weststrate, C.J.; Andersen, J.N.; Seitsonen, A.P.; Over, H. Stable deacon process for HCl oxidation over RuO_2. *Angew. Chem. Int. Ed.* **2008**, *47*, 2131–2134. [CrossRef] [PubMed]
40. Shi, W.; Liu, X.; Zeng, J.; Wang, J.; Wei, Y.; Zhu, T. Gas-solid catalytic reactions over ruthenium-based catalysts. *Chin. J. Catal.* **2016**, *37*, 1181–1192. [CrossRef]
41. Xiang, G.; Shi, X.; Wu, Y.; Zhuang, J.; Wang, X. Size effects in atomic-level epitaxial redistribution process of RuO_2 over TiO_2. *Sci. Rep.* **2012**, *2*, 801. [CrossRef] [PubMed]
42. Mondelli, C.; Amrute, A.P.; Krumeich, F.; Schmidt, T.; Pérez-Ramírez, J. Shaped RuO_2/SnO_2-Al_2O_3 Catalyst for Large-Scale Stable Cl_2 Production by HCl Oxidation. *Hemcatchem* **2011**, *3*, 657–660. [CrossRef]
43. López, N.; Gómez-Segura, J.; Marín, R.P.; Pérez-Ramírez, J. Mechanism of HCl oxidation (Deacon process) over RuO_2. *J. Catal.* **2008**, *255*, 29–39. [CrossRef]
44. Okal, J.; Zawadzki, M. Catalytic combustion of butane on Ru/γ-Al_2O_3 catalysts. *Appl. Catal. B Environ.* **2009**, *89*, 22–32. [CrossRef]
45. Kamiuchi, N.; Mitsui, T.; Muroyama, H.; Matsui, T.; Kikuchi, R.; Eguchi, K. Catalytic combustion of ethyl acetate and nano-structural changes of ruthenium catalysts supported on tin oxide. *Appl. Catal. B Environ.* **2010**, *97*, 120–126. [CrossRef]
46. Okal, J.; Zawadzki, M.; Tylus, W. Microstructure characterization and propane oxidation over supported Ru nanoparticles synthesized by the microwave-polyol method. *Appl. Catal. B Environ.* **2011**, *101*, 548–559. [CrossRef]
47. Okal, J.; Zawadzki, M. Combustion of propane over novel zinc aluminate-supported ruthenium catalysts. *Appl. Catal. B Environ.* **2011**, *105*, 182–190. [CrossRef]
48. Debecker, D.P.; Farin, B.; Gaigneaux, E.M.; Sanchez, C.; Sassoye, C. Total oxidation of propane with a nano-RuO_2/TiO_2 catalyst. *Appl. Catal. A Gen.* **2014**, *481*, 11–18. [CrossRef]
49. Liu, X.; Zeng, J.; Shi, W.; Wang, J.; Zhu, T.; Chen, Y. Catalytic oxidation of benzene over ruthenium–cobalt bimetallic catalysts and study of its mechanism. *Catal. Technol.* **2016**, *7*, 213–221. [CrossRef]
50. Dai, Q.; Bai, S.; Wang, J.; Li, M.; Wang, X.; Lu, G. The effect of TiO_2 doping on catalytic performances of Ru/CeO_2 catalysts during catalytic combustion of chlorobenzene. *Appl. Catal. B Environ.* **2013**, *142*, 222–233. [CrossRef]
51. Dai, Q.; Bai, S.; Wang, Z.; Wang, X.; Lu, G. Catalytic combustion of chlorobenzene over Ru-doped ceria catalysts. *Appl. Catal. B Environ.* **2012**, *126*, 64–75. [CrossRef]
52. Miranda, B.; Díaz, E.; Ordóñez, S.; Díez, F.V. Catalytic combustion of trichloroethene over Ru/Al_2O_3: Reaction mechanism and kinetic study. *Catal. Commun.* **2006**, *7*, 945–949. [CrossRef]

53. Liu, X.; Zeng, J.; Wang, J.; Shi, W.; Zhu, T. Catalytic oxidation of methyl bromide using ruthenium-based catalysts. *Catal. Sci. Technol.* **2016**, *6*, 4337–4344. [CrossRef]
54. Dai, Q.; Bai, S.; Wang, X.; Lu, G. Catalytic combustion of chlorobenzene over Ru-doped ceria catalysts: Mechanism study. *Appl. Catal. B Environ.* **2013**, *129*, 580–588. [CrossRef]
55. Sreethawong, T.; Sukjit, D.; Ouraipryvan, P.; Schwank, J.W.; Chavadej, S. Oxidation of Oxygenated Volatile Organic Compound Over Monometallic and Bimetallic Ru-Au Catalysts. *Catal. Lett.* **2010**, *138*, 160–170. [CrossRef]
56. Aouad, S.; Saab, E.; Abi-Aad, E.; Aboukaïs, A. Study of the Ru/Ce system in the oxidation of carbon black and volatile organic compounds. *Kinet. Catal.* **2007**, *48*, 835–840. [CrossRef]
57. Jodaei, A.; Salari, D.; Niaei, A.; Khatamian, M.; Çaylak, N. Preparation of Ag-M (M: Fe, Co and Mn)-ZSM-5 bimetal catalysts with high performance for catalytic oxidation of ethyl acetate. *Environ. Technol.* **2011**, *32*, 395–406. [CrossRef] [PubMed]
58. Barakat, T.; Idakiev, V.; Cousin, R.; Shao, G.S.; Yuan, Z.Y.; Tabakova, T.; Siffert, S. Total oxidation of toluene over noble metal based Ce, Fe and Ni doped titanium oxides. *Appl. Catal. B Environ.* **2014**, *146*, 138–146. [CrossRef]
59. Xie, S.; Deng, J.; Zang, S.; Yang, H.; Guo, G.; Arandiyan, H.; Dai, H. Au-Pd/3DOM Co_3O_4: Highly active and stable nanocatalysts for toluene oxidation. *J. Catal.* **2015**, *322*, 38–48. [CrossRef]
60. Darif, B.; Ojala, S.; Pirault-Roy, L.; Bensitel, M.; Brahmi, R.; Keiski, R.L. Study on the catalytic oxidation of DMDS over Pt-Cu catalysts supported on Al_2O_3, $AlSi_{20}$ and SiO_2. *Appl. Catal. B Environ.* **2016**, *181*, 24–33. [CrossRef]
61. Wang, X.; Stöver, J.R.; Zielasek, V.; Altmann, L.; Thiel, K.; Al-Shamery, K.; Bäumer, M.; Borchert, H.; Parisi, J.R.; Kolny-Olesiak, J. Colloidal synthesis and structural control of PtSn bimetallic nanoparticles. *Langmuir* **2011**, *27*, 11052–11061. [CrossRef] [PubMed]
62. Zhao, S.; Li, K.; Jiang, S.; Li, J. Pd-Co based spinel oxides derived from Pd nanoparticles immobilized on layered double hydroxides for toluene combustion. *Appl. Catal. B Environ.* **2016**, *181*, 236–248. [CrossRef]